PHYSICAL REVIEW B **91**, 205125 (2015)

Two kinds of in-plane resistivity anisotropy in $Fe_{1+\delta}Te$ ($\delta = 0.09$) as seen via synchrotron radiation x-ray diffraction and *in situ* resistivity measurements

Taro Nakajima,[1,*] Tadashi Machida,[1,†] Hironori Kariya,[1] Daiki Morohoshi,[1] Yuichi Yamasaki,[2,†] Hironori Nakao,[2] Kazuto Hirata,[3] Takashi Mochiku,[3] Hiroyuki Takeya,[4] Setsuo Mitsuda,[1] and Hideaki Sakata[1]

[1]*Department of Physics, Faculty of Science, Tokyo University of Science, Tokyo 162-8601, Japan*

[2]*Condensed Matter Research Center and Photon Factory, Institute of Materials Structure Science, High Energy Accelerator Research Organization, Tsukuba 305-080, Japan*

[3]*Superconducting Properties Unit, National Institute for Materials Science, 1-2-1 Sengen, Tsukuba, Ibaraki 305-0047, Japan*

[4]*Superconducting Wires Unit, National Institute for Materials Science, 1-2-1 Sengen, Tsukuba, Ibaraki 305-0047, Japan*

(Received 2 February 2015; revised manuscript received 5 May 2015; published 22 May 2015)

We have investigated correlation between structural and electronic anisotropies in a parent compound of Fe-chalcogenide superconductor $Fe_{1+\delta}Te$ with $\delta = 0.09$ by means of synchrotron x-ray diffraction and *in situ* in-plane resistivity anisotropy measurements with uniaxial stress applied along a tetragonal *a* axis. This system is known to exhibit a tetragonal-to-monoclinic structural transition at $T_S \sim 60$ K. We have confirmed that the in-plane resistivity anisotropy in the low-temperature monoclinic phase is attributed to the asymmetry in volume fractions of the monoclinic domains, as was suggested in a previous study [Jiang *et al.*, Phys. Rev. B **88** 115130 (2013)]. On the other hand, we found another in-plane resistivity anisotropy above T_S. The present x-ray diffraction and resistivity anisotropy measurements have revealed that this anisotropy is not due to an onset of the low-temperature monoclinic phase but to the lattice softening enhanced toward T_S. As one of the possibilities, we suggest that the orbital fluctuation contributes to the lattice softening and the resistivity anisotropy above T_S.

DOI: 10.1103/PhysRevB.91.205125 PACS number(s): 74.70.Xa, 72.15.−v, 74.62.Fj, 78.70.Ck

I. INTRODUCTION

Fe-based superconductors (FeSCs) and their parent compounds have been intensively investigated since their discovery [1,2]. Similarly to the high-T_C cuprates, most of the FeSCs have square lattices of the magnetic ions (Fe^{2+}), and also exhibit antiferromagnetic orders in their parent phases. It is also known that the antiferromagnetic orders are suppressed by electron or hole doping, or even by isovalent substitution [1–5]. In the vicinity of the critical point where the antiferromagnetic long-range order vanishes, the superconducting state is often observed to emerge. These similarities imply that the spin fluctuation, which is considered to be the key to the origin of the high-T_C superconductivity in the cuprates, also plays an important role in the FeSCs.

On the other hand, the FeSCs have several remarkable differences from the cuprates. One of them is the existence of symmetry-lowering structural transitions in their parent compounds. For instance, $BaFe_2As_2$, which is one of the most enthusiastically investigated systems, exhibits a tetragonal-to-orthorhombic structural transition, which is followed by the antiferromagnetic order [6]. Interestingly, this structural transition is accompanied by large resistivity anisotropy in the square-lattice plane. Chu *et al.* have demonstrated that the magnitude of the in-plane resistivity anisotropy is significantly enhanced by substituting Co ions for the Fe sites [7]; specifically, the resistivity along the orthorhombic *b* axis becomes twice as large as that along the orthorhombic *a* axis in the vicinity of the superconducting dome. Moreover, Kasahara *et al.* have recently reported x-ray diffraction and magnetic torque measurements on $BaFe_2(As_{1-x}P_x)_2$, suggesting that the fourfold rotational symmetry of the lattice is broken even above T_S due to the anisotropic electronic correlation called "(electronic) nematic order" [8]. The emergence of the anisotropic electronic state above T_S has been also suggested in the recent linear x-ray dichroism [9] and electronic Raman spectroscopy [10] experiments. These results suggest that the orbital and lattice degrees of freedom are relevant to the phase transitions in this system, implying that their fluctuations might also contribute to the pairing mechanism of the superconductivity.

The breaking of the fourfold rotational symmetry in the *ab* plane naturally leads to a multidomain state in which (at least) two domains with different orientations coexist. Therefore the electronic anisotropy is often hidden behind the domain structure. In some of the previous studies, uniaxial stress was applied in the *ab* plane in order to obtain a "single-domain" state [7,11]. However, the application of the uniaxial stress may introduce an "extrinsic" anisotropy. In fact, the previous neutron diffraction study has demonstrated that the magnetic phase transition temperature is readily shifted toward higher values by applying small uniaxial stress [12]. To quantitatively discuss the correlation between the electronic and structural anisotropies in these systems, it is important to measure both of them simultaneously. In the present study, we thus performed synchrotron radiation x-ray diffraction and *in situ* resistivity anisotropy measurements on $Fe_{1+\delta}Te$, which is a parent compound of Fe-chalcogenide superconductors.

$Fe_{1+\delta}Te$ has the simplest crystal structure among the family of the FeSCs [13]. Similarly to the other FeSCs, this system also has a tetragonal crystal structure, which contains anti-PbO-type FeTe layers, as shown in Figs. 1(a) and 1(b). These

*Present address: Center for Emergent Matter Science, RIKEN, Saitama 351-0198, Japan; taro.nakajima@riken.jp

†Present address: Center for Emergent Matter Science, RIKEN, Saitama 351-0198, Japan.

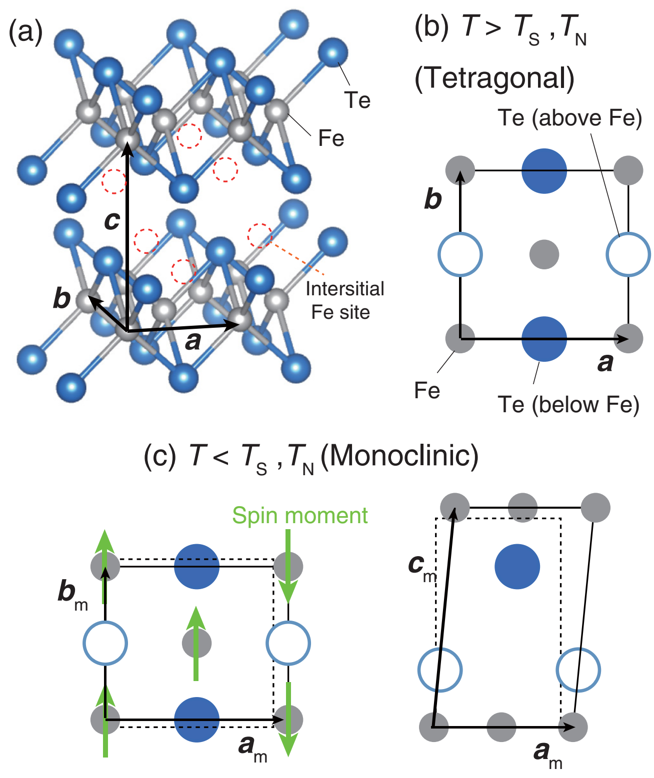

FIG. 1. (Color online) (a) Crystal structure of $Fe_{1+\delta}Te$. Dotted circles show the positions of the interstitial Fe ions. Schematics of the (b) tetragonal (c) and monoclinic unit cells of $Fe_{1+\delta}Te$. Green (gray) arrows in (c) show the directions of the magnetic moments on each Fe site.

layers are stacked along the c axis and are loosely coupled via van der Waals interaction. In addition, this system contains interstitial Fe ions between the FeTe layers. It is known that the amount of interstitial Fe ions affects magnetic orders in this system [13]. Bao *et al.* have reported that $Fe_{1+\delta}Te$ exhibits a commensurate bicollinear antiferromagnetic order in the excess-Fe concentration region of $0 < \delta < 0.1$, while it shows an incommensurate magnetic order in the region of $\delta > 0.1$ [14]. $Fe_{1+\delta}Te$ with $\delta = 0.09$, to be investigated here, exhibits the former magnetic order below the magnetic transition temperature of $T_N \sim 60$ K. Unlike the other FeSCs, this magnetic transition temperature exactly coincides with the structural transition temperature T_S. Moreover, in $Fe_{1+\delta}Te$ with $\delta = 0.09$, the original tetragonal structure turns into not orthorhombic structure but into monoclinic structure below T_S. In Figs. 1(b) and 1(c), we show definitions of the tetragonal and monoclinic bases. To distinguish between these bases, we add a subscript "m" when referring to basis, reflections, and reciprocal lattice vectors in the monoclinic notation. Note that the a (b) and a_m (b_m) axes are parallel to each other in this system, while in the other FeSCs, such as $BaFe_2As_2$, the orthorhombic a axis is parallel to the tetragonal [110] direction.

Quite recently, Jiang *et al.* [15] and Liu *et al.* [16] performed resistivity measurements on $Fe_{1+\delta}Te$ with uniaxial stress. They have shown that the application of uniaxial stress induces large in-plane resistivity anisotropy below T_S. However, the degree of detwinning was not checked in their experiments. Note that in the previous studies on the uniaxial-stress effects in the 122 systems, the degree of detwinning was directly observed by means of x-ray diffraction techniques [7,11]. Specifically, they observed that tetragonal HHL reflections split into two peaks, which are indexed as $H0L$ and $0HL$ in the orthorhombic notation, below T_S. They revealed that the application of uniaxial-stress results in a remarkable difference between the intensities of the split reflections, which are proportional to the volume fractions of the two orthorhombic domains with different orientations. On the other hand, in $Fe_{1+\delta}Te$ ($\delta = 0.09$), the tetragonal-to-monoclinic structural transition results in four monoclinic domains, as shown later in Fig. 3(f), and therefore the domain structure under applied uniaxial stress is not trivial. In the present study, we have identified the monoclinic domain structure by means of the x-ray diffraction measurements and have also revealed the quantitative relationship between volume fractions of the monoclinic domains and the in-plane resistivity anisotropy below T_S.

As for the high-temperature tetragonal phase, a small in-plane resistivity anisotropy was observed just above T_S in the previous studies [15,16]. Although this small anisotropy might be indicative of the electronic nematic order similar to that reported in the 122-type FeSCs [8], this point has not been investigated in detail, so far. We have thus also investigated whether the subtle and spontaneous symmetry breaking occurs in the tetragonal phase of $Fe_{1+\delta}Te$, by means of the x-ray diffraction and *in situ* resistivity anisotropy measurements.

II. EXPERIMENTS

Single crystals of $Fe_{1+\delta}Te$ with $\delta = 0.09$ of nominal composition were grown by melting-growth technique and were cut into rectangular shapes with the largest surface normal to the c axis. The dimensions of the samples were typically $3 \times 3 \times 1$ mm^3. The synchrotron radiation x-ray diffraction measurements were carried out at beamline BL-3A at the Photon Factory of the High Energy Accelerator Research Organization, Tsukuba, Japan. The energy of the incident x ray was tuned to 14 keV. We have employed a top-loading-type uniaxial-stress insert used in Refs. [17–19]. The insert was loaded into a ^{4}He-flow-type cryomagnet installed at BL-3A. As shown in Fig. 2(a), the sample was placed between the ZrO_2 pistons. Here, we introduce a Cartesian coordinate, xyz, as shown in Fig. 2(b), and define the tetragonal b axis to be parallel to the z direction, although the a and b axes are equivalent to each other in the tetragonal lattice. The uniaxial compressive stress (σ) was applied along the tetragonal b axis, namely, the z direction.

The *in situ* resistivity measurements were also performed in the x-ray diffraction measurements. We employed the Montgomery method [20,21] to observe the in-plane resistivity anisotropy. Four gold electrodes were formed at the corners on the c plane of the sample, as shown in Fig. 2(b). These electrodes were connected to a current source and a nanovoltmeter through a switcher. By switching the terminals for the current and voltage as shown in Figs. 2(c) and 2(d), we can measure the resistivity along the a and b directions.

The x-ray beam was diffracted on the c and a planes for measuring the $H0L$ ($L \neq 0$) and $H00$ reflections, respectively, as shown in Figs. 2(e) and 2(f). In the former configuration,

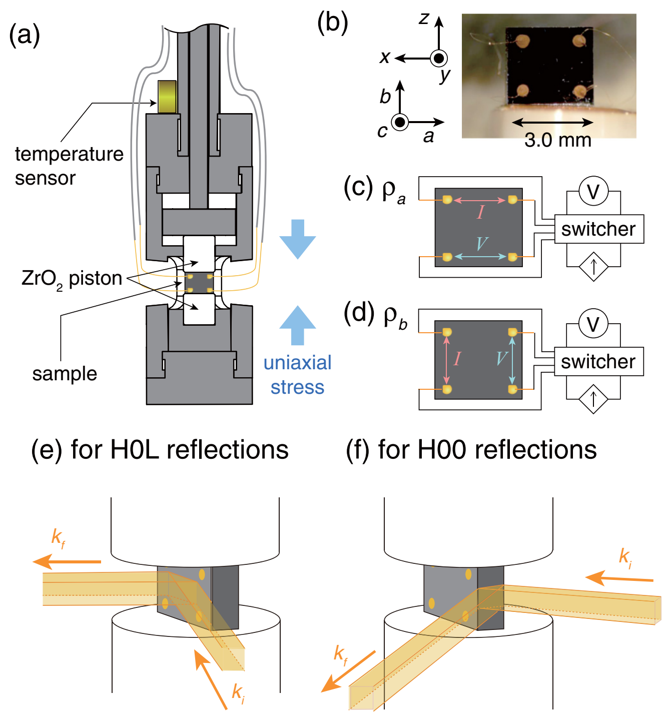

FIG. 2. (Color online) (a) A schematic drawing of the uniaxial-stress cell. (b) A picture of the sample used for the present x-ray and *in situ* resistivity measurements. Schematics showing the configurations for the measurements of (c) ρ_a and (d) ρ_b for the Montgomery method. Schematics showing the diffraction paths for the measurements of (e) the $H0L$ ($L \neq 0$) and (f) $H00$ reflections.

we can directly observe the structural anisotropy in the area just between the electrodes.

We also performed offline in-plane resistivity anisotropy measurements under various uniaxial stresses using four different samples of $Fe_{1+\delta}Te$ ($\delta = 0.09$).

III. RESULTS AND DISCUSSION

A. Identification of the monoclinic domain structure below T_S

As mentioned in the Introduction, this system is known to exhibit the tetragonal-to-monoclinic structural transition at T_S. Owing to the original fourfold rotational symmetry of the tetragonal structure, there exist four monoclinic domains below T_S. We found that the fundamental reflections split into several peaks below T_S, as shown in Figs. 3(a)–3(d); the $H0L$ reflections with $L \neq 0$ split into four peaks, while the $H00$ reflections are split into two peaks. These reflections are successfully indexed using monoclinic lattice constants reported in the previous study on $Fe_{1+\delta}Te$ with $\delta = 0.076$ [14].

The splitting of $00L$ reflections indicates that the $c^*_{\rm m}$ axes in each monoclinic domain are inclined from the tetragonal c^* direction. On the other hand, the $a^*_{\rm m}$ and $b^*_{\rm m}$ axes remain parallel to the tetragonal a^* or b^* axis, as shown in Fig. 3(a). These results show that in real space, the $c_{\rm m}$ axes of the four monoclinic domains are parallel to each other, while the $a_{\rm m}$ axes are slightly inclined from the tetragonal a or b axis, as shown in Fig. 3(f). Because it is impossible to fill up the space with the four kinds of monoclinic unit cells, a structural discrepancy must exist on the monoclinic domain walls. The schematic domain structure shown in Fig. 3(f) suggests that the structural discrepancy appears mainly on the domain walls perpendicular to the c axis, on which the out-of-plane Te-Te

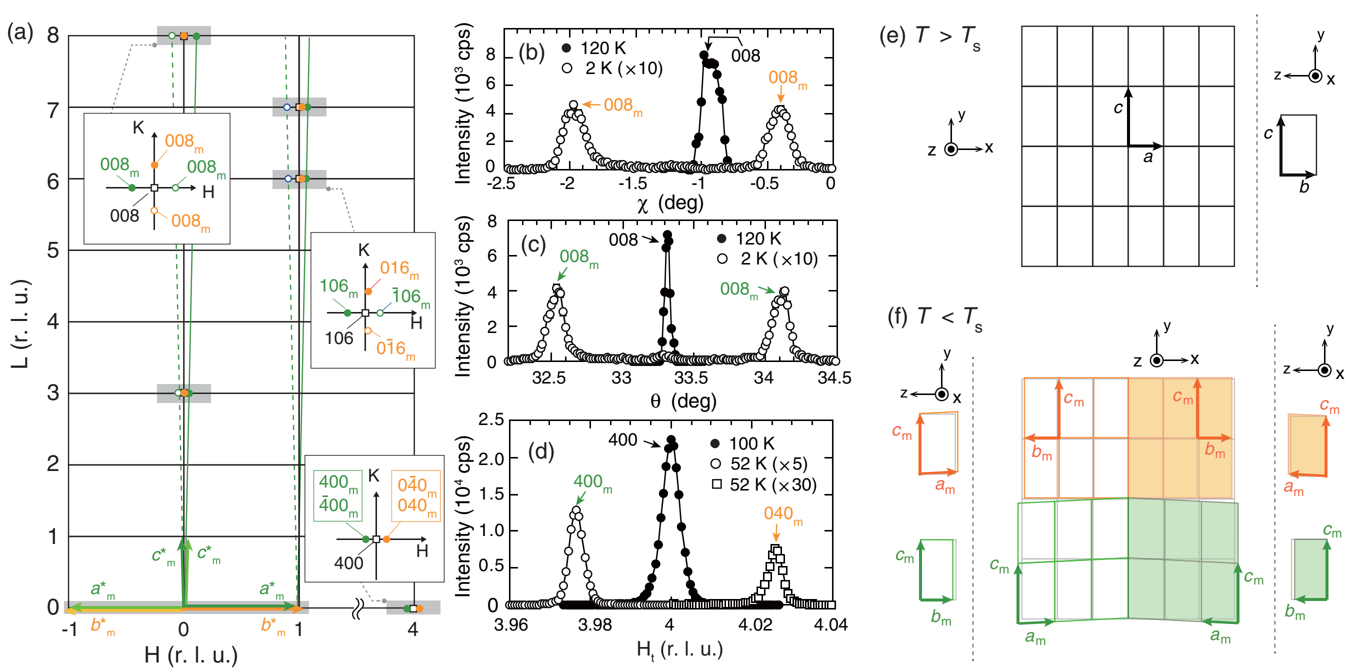

FIG. 3. (Color online) (a) The reciprocal lattice map of the $(H,0,L)$ plane. We observed the splitting of the 200, 400, 106, 107, 003, and 008 reflections. Typical diffraction profiles of the 008 reflection measured along (b) χ direction (K direction) and (c) θ direction (H direction), and (d) those of the 400 reflection along the $(H,0,0)$ direction, above and below T_S. Schematics showing (e) the tetragonal lattice above T_S and (f) the formation of the four monoclinic domains below T_S.

bondings have to be stretched (or cut). On the other hand, these domains can be relatively smoothly connected with each other along the a and b directions, although the bonding angle should be slightly altered at the domain walls. This is consistent with the fact that the out-of-plane Te-Te bonding, which is mediated by the van der Waals force, is considerably weak as compared with the in-plane bondings.

B. In-plane resistivity anisotropy due to the monoclinic domain structure below T_S

To elucidate the quantitative relationship between the in-plane resistivity anisotropy and volume fractions of the four monoclinic domains, we measured intensities of the split reflections in the monoclinic phase, and also performed the *in situ* in-plane resistivity anisotropy measurements in zero uniaxial stress and under applied σ of 5 MPa. Figures 4(a) and 4(b) shows temperature variations of ρ_a and ρ_b measured upon cooling under $\sigma = 0$ and 5 MPa, respectively. Under zero uniaxial stress, the in-plane resistivity is nearly isotropic both above and below T_S. On the other hand, under $\sigma = 5$ MPa, a large in-plane resistivity anisotropy was observed below T_S; specifically, ρ_b is smaller than ρ_a. These results are consistent with previous studies [15,16].

Just after each of the resistivity measurements, we measured x-ray intensity maps in the vicinity of the tetragonal reciprocal lattice point of (1,0,6) at 2 K. In zero uniaxial stress, the intensities of the four split reflections are comparable to each other, as shown in Figs. 4(c) and 4(d). This indicates that the volume fractions of the four monoclinic domains are nearly equal to each other. By contrast, under applied uniaxial stress, the intensities of the 106_m, $\bar{1}06_\mathrm{m}$ reflections were significantly enhanced, while those of the other two reflections were reduced, as shown in Figs. 4(e) and 4(f), respectively. This apparently shows that the application of the uniaxial stress suppresses the monoclinic domains whose a^*_m axes are parallel

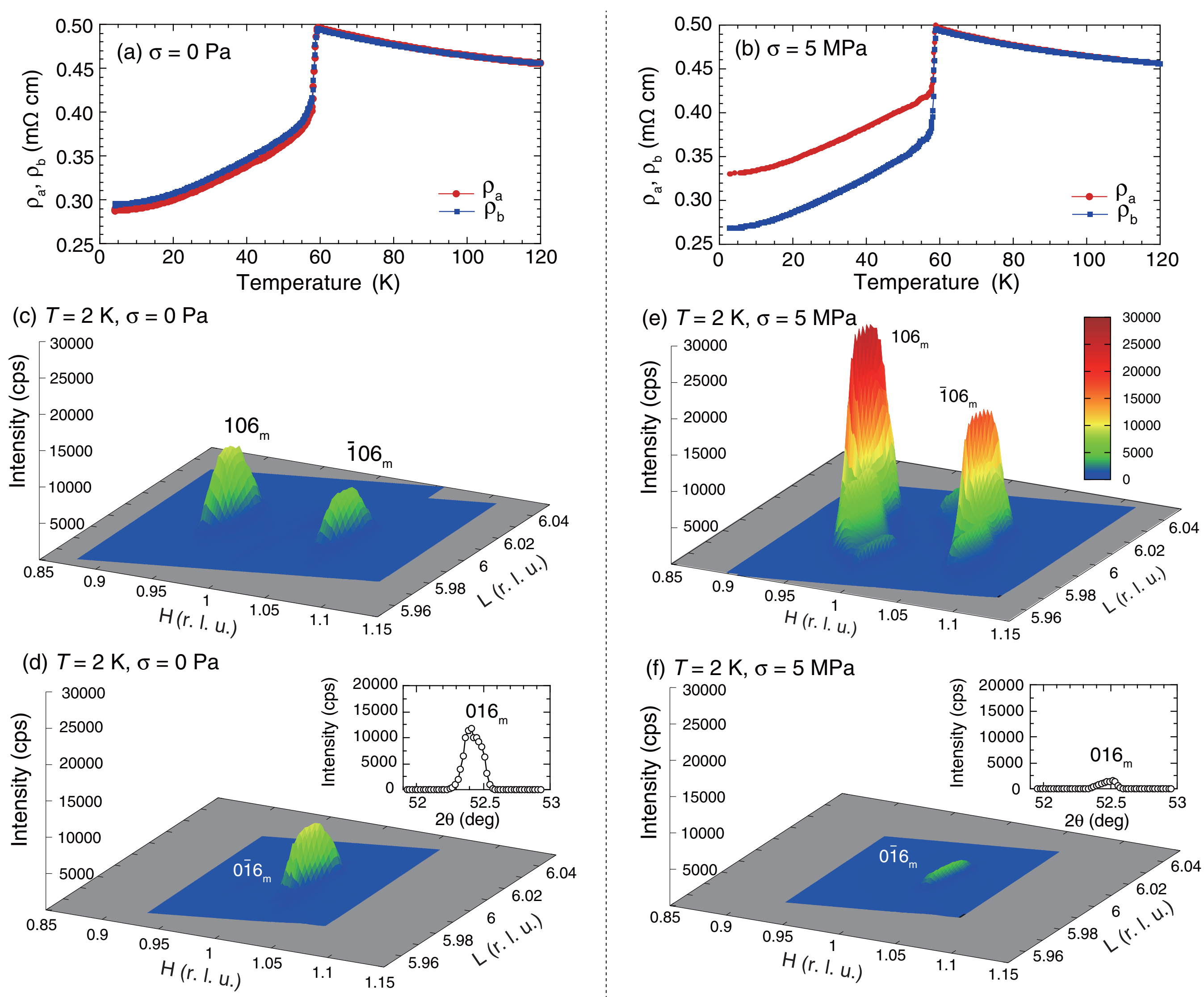

FIG. 4. (Color online) The temperature variations of ρ_a and ρ_b measured on cooling (a) in zero uniaxial stress and (b) under applied σ of 5 MPa. The x-ray intensity maps near (c) the 106_m and $\bar{1}06_\mathrm{m}$ reflections and (d) the $0\bar{1}6_\mathrm{m}$ reflection measured subsequent to the resistivity measurements shown in (a). The x-ray intensity maps measured after the resistivity measurement of (b) are shown in (e) and (f). Insets shown in (d) and (f) are the profiles of the θ-2θ scans for the 016_m reflection.

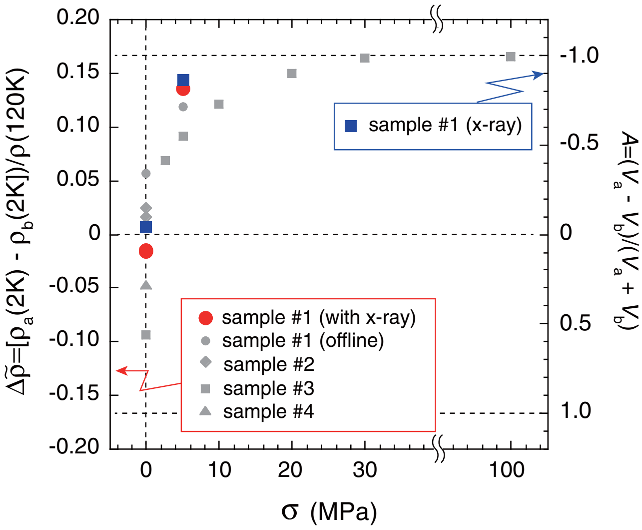

FIG. 5. (Color online) The σ dependencies of the asymmetry in volume fractions of the monoclinic domains and the normalized in-plane resistivity anisotropy measured for several different samples. Colored (large) symbols show the results of the x-ray diffraction and *in situ* resistivity measurements. Gray (small) symbols show the results of the offline resistivity measurements. Note that sample no. 1 was used in both the x-ray diffraction and offline resistivity measurements.

to the uniaxial stress. This is consistent with the fact that the a_{m} and b_{m} axes elongate and contract, as compared to the a and b axes in the tetragonal phase, respectively [14].

Hereafter, we refer to the two domains whose a_{m} axes lie along the applied stress as "$\sigma||a$ domains" and to the other two domains as "$\sigma||b$ domains." The volume fractions of the $\sigma||a$ and $\sigma||b$ domains, V_a and V_b, can be estimated as follows;

$$V_a \propto I_{016_{\mathrm{m}}} + I_{0\bar{1}6_{\mathrm{m}}}, \tag{1}$$

$$V_b \propto I_{106_{\mathrm{m}}} + I_{\bar{1}06_{\mathrm{m}}}, \tag{2}$$

where $I_{hkl_{\mathrm{m}}}$ is the integrated intensity measured by a θ-2θ scan for the reflection indexed as hkl_{m}. In Fig. 5 we show a comparison between asymmetry in volume fractions, $A = (V_a - V_b)/(V_a + V_b)$, and normalized in-plane resistivity anisotropy, $\Delta\tilde{\rho} = [\rho_a(2\ \mathrm{K}) - \rho_b(2\ \mathrm{K})]/\rho_a(120\ \mathrm{K})$. In addition to the results of the *in situ* resistivity measurements, we have also plotted the σ variations of $\Delta\tilde{\rho}$ obtained from the offline resistivity measurements using several different samples. We found that $\Delta\tilde{\rho}$ saturates at around 0.165 in the high-uniaxial-stress limit. By scaling the saturation value of $\Delta\tilde{\rho}$ to $A = -1$, the values of $\Delta\tilde{\rho}$ and A obtained in the *in situ* measurements are in good agreement with each other. This demonstrates that the in-plane resistivity anisotropy below T_{S} is determined by the asymmetry in the volume fractions of the monoclinic domains, which can be controlled by the application of relatively weak uniaxial stress (5 ∼ 20 MPa).

As for the origin of the in-plane resistivity anisotropy below T_{S}, Jiang *et al.* have suggested that the bicollinear-type magnetic structure, which has antiferromagnetic and ferromagnetic spin arrangements along the a_{m} and b_{m} axes, respectively, yields an additional energy barrier only for the electrons hopping along the a axis because of strong Hund coupling [15]. This interpretation naturally suggests that the hopping probability along the a axis decreases with decreasing temperature and that the difference between ρ_a and ρ_b is enhanced at low temperatures. However, our present results, as well as the previous results [15,16], show that the difference between $\rho_a(T)$ and $\rho_b(T)$ is not in the slope but in the residual resistivity. In fact, Liu *et al.* have argued that the interstitial Fe ions act as a scattering center with "anisotropic" scattering potential and consequently lead to the difference in residual resistivity [16]. This agrees with recent scanning tunneling microscopy/spectroscopy observations by Machida *et al.* [22], revealing the spatial anisotropy of the density of states in the vicinity of the interstitial Fe ions. Therefore we have considered that the impurity-scattering scenario is more plausible than the Hund-coupling scenario.

C. Structural and resistivity anisotropy above T_{S}

To investigate the structural and electronic anisotropies above T_{S}, we simultaneously measured temperature variations of the x-ray diffraction profile of the 400 reflection and the in-plane resistivity anisotropy. Figure 6(a) shows the temperature variation of the θ-2θ scan profile of the 400 reflection measured on cooling in zero uniaxial stress. At each measuring temperature, we refined the peak position before measuring the θ-2θ scan. We found that the peak position, intensity, and linewidth were nearly independent of temperature above T_{S}, as seen in Fig. 6(a) and its inset, suggesting that the system keeps the tetragonal symmetry above T_{S}. This is consistent with the results of the *in situ* resistivity measurement shown in Fig. 6(d); the normalized resistivity anisotropy does not show remarkable temperature dependence in the tetragonal phase.

Around $T = 60$ K, the 400 reflection suddenly disappears and instead, two reflections, namely, 400_{m} and 040_{m}, appear. Note that in this paper, we defined T_{S} as the temperature at which the 400_{m} or 040_{m} reflections start to emerge, and that is estimated to be 60 K at 0 Pa. Below T_{S}, we found that the intensities of these two reflections were not equal to each other. This might be due to the residual stress in the sample [23]. In fact, we observed a finite resistivity anisotropy below T_{S}, as shown in Fig. 6(d). The positive sign of $(\rho_a - \rho_b)/\rho(90\ \mathrm{K})$ shows that the volume fraction of the $\sigma||b$ domains was larger than that of the $\sigma||a$ domains, and agrees with the observed asymmetry between the intensities of the 400_{m} and 040_{m} reflections.

Figure 6(b) shows the temperature dependence of the θ-2θ scan profile measured on cooling under applied σ of 54 MPa. We found that the application of σ shifts T_{S} toward higher values. This can be interpreted in that the application of the "compressive" uniaxial stress induces the monoclinic phase, which has a smaller lattice constant along the uniaxial stress than the tetragonal phase, above the original transition temperature. In addition, above T_{S} we found that the peak position of the 400 reflection gradually shifts toward a lower angle with decreasing temperature. This indicates that the tetragonal structure was distorted by the application of the uniaxial stress, and the degree of the distortion was gradually enhanced toward T_{S}. Note that near T_{S}, the 400 reflection

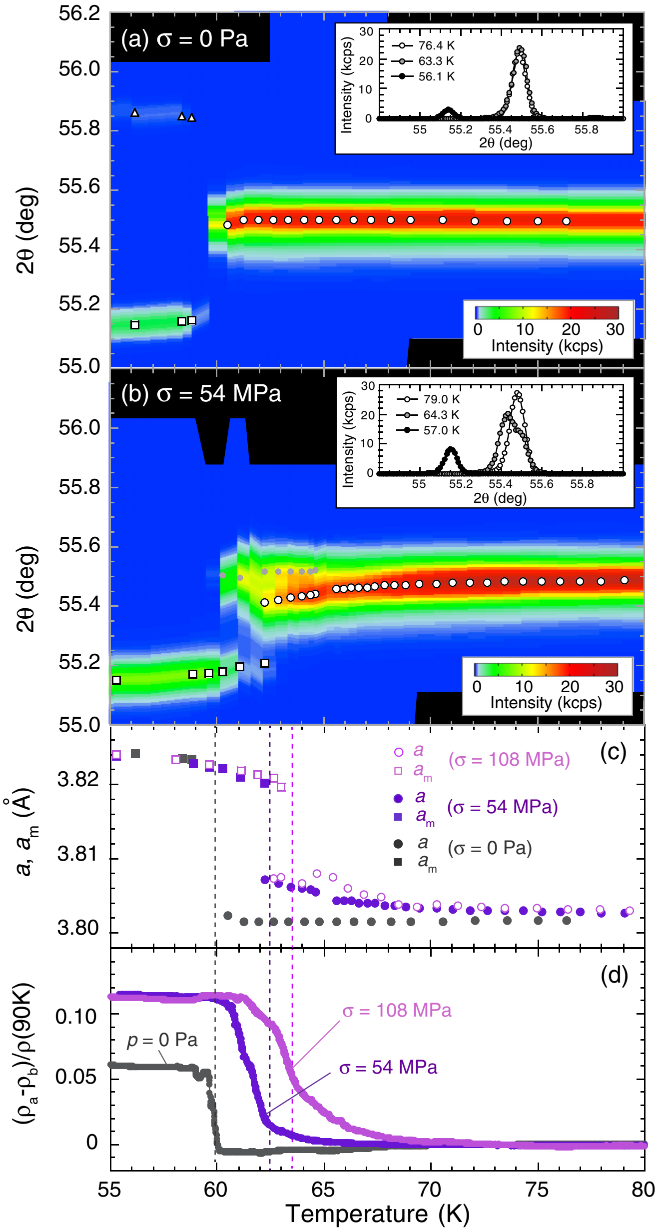

FIG. 6. (Color online) Contour maps showing the temperature dependencies of the x-ray diffraction profiles for the 400 reflection measured by θ-2θ scans (a) in zero uniaxial stress and (b) under applied $\sigma = 54$ MPa, on cooling. Open circles, squares, and triangles show the peak positions of the 400, 400_m, and 040_m reflections, respectively. The small shoulder of the 400 reflection, which might be due to the spatial inhomogeneity of the applied stress, is shown by gray-filled circles. Insets show typical profiles of θ-2θ scans at several temperatures. Temperature variations of (c) the lattice constants a and a_m and (d) the in-plane resistivity anisotropy measured under $\sigma = 0, 54$ and 108 MPa upon cooling.

had a small shoulder, as seen in the inset of Fig. 6(b). The position of the shoulder peak at each temperature is shown by gray-filled circles in Fig. 6(b). The small shoulder peak remained down to ~60 K, and its position was close to that of the 400 reflection in zero uniaxial stress. This suggests that the applied uniaxial stress was not homogeneous on the surface of the sample (probably due to the imperfect contact between the sample and pistons), and therefore some part of the sample was not sufficiently pressurized. Nevertheless, the 040_m reflection, which corresponds to the $\sigma \parallel a$ domain, was not observed under applied σ of 54 MPa. We thus consider that the effective stress for most of the sample was 50~60 MPa and that for the other part was at least 5~10 MPa, according to the σ dependence of the asymmetry of the volume fractions shown in Fig. 5.

In Fig. 6(c), we show temperature dependencies of the lattice constant a (a_m) calculated from the temperature dependencies of the 400 (400_m) reflection measured under $\sigma = 0, 54$ and 108 MPa. This shows that the lattice constant shows remarkable σ dependence in the tetragonal phase, particularly near T_S. In contrast, it is rather insensitive to σ in the monoclinic phase.

To identify the symmetry of the distorted crystal structure above T_S under applied σ, we also measured θ scans of the 008 reflection. As mentioned in the previous section, the 008 reflection splits into two (or at most four) reflections when the system undergoes the tetragonal-to-monoclinic structural transition. However, the 008 reflection does not show the splitting above T_S, even under applied $\sigma = 108$ MPa [24], while it was found to split below T_S, as shown in Figs. 7(a) and 7(b), respectively. This indicates that although the original tetragonal symmetry should be broken by the application of σ, the σ-induced lattice distortion above T_S is distinct from an onset of the low-temperature monoclinic phase. Instead, we suggest the possibility that the crystal structure is gradually softened with decreasing temperature toward T_S, and the application of σ along the b axis results in the lattice expansion along the a (and c) direction(s).

It should be mentioned here that similar elastic softenings have been observed in the 122-type FeSCs by means of resonant ultrasound spectroscopy [25,26]. Although we could not deduce the temperature variations of elastic constants of $Fe_{1+\delta}Te$ from the present results, we suggest that a similar

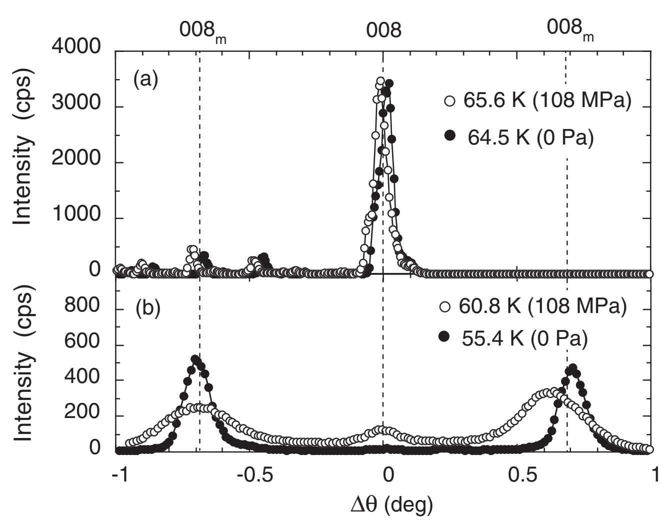

FIG. 7. The x-ray diffraction profiles of the 008 reflection measured by the θ scans (a) above T_S and (b) below T_S. Filled and open symbols correspond to the data measured in zero uniaxial stress and under applied uniaxial stress of 108 MPa, respectively.

kind of softening also occurs in the 11 system and is common to the structural transitions in the FeSCs.

We also found that the resistivity anisotropy also starts to grow above T_S under applied σ, as shown in Fig. 6(d). On the basis of the present x-ray results, we consider that the evolution of the resistivity anisotropy originates from the lattice distortion due to the large softening and the application of σ. The strong correlation between the structural instability and in-plane resistivity anisotropy might be indicative of orbital fluctuation, which may affect both the structural and electronic anisotropy near T_S. In fact, Turner *et al.* have theoretically predicted the existence of an orbital order in the monoclinic phase of this system [27].

An alternative interpretation for the resistivity anisotropy above T_S is that the σ-induced distortion simply leads to the anisotropic density of state near the interstitial Fe ions, which may give rise to the anisotropic impurity scattering similarly to the case of the anisotropy below T_S. Even in this interpretation, the lattice softening enhanced near T_S is essential to explain the temperature dependence of the resistivity anisotropy above T_S.

It is worth mentioning that in the present measurements, we could not observe the "spontaneous" breaking of the fourfold rotational symmetry above T_S, while the several previous studies on the 122-type FeSCs have argued the existence of the critical temperature at which the electronic nematic order parameter [8] or the subtle orbital order [9] starts to grow. Specifically, Kasahara *et al.* have reported that the peak width of the $\underline{1}400$ reflection starts to increase at the nematic transition temperature [8], while the present results show that the width of the 400 reflection is nearly independent of temperature in zero uniaxial stress, as shown in Fig. 6(a) and its inset [28]. Although the present results have suggested that the system exhibits the lattice softening, which may imply the existence of the orbital fluctuation, it seems to gradually and monotonically grow toward T_S. This is rather consistent with the electroelasticity measurements on $Ba(Fe_{1-x}Co_x)_2As_2$ by Chu *et al.* [29]; they have reported that the electronic nematic susceptibility, which is defined as the susceptibility for a strain-induced change in resistivity, gradually grows from the higher temperature and diverges near T_S. The preset results suggest that the spontaneous nematic order scenario is not the case and instead, the divergent nematic susceptibility may exist in the 11 system.

IV. SUMMARY

We have investigated the correlations between the structural and electronic anisotropies above and below T_S in $Fe_{1+\delta}Te$ with $\delta = 0.09$ by means of synchrotron x-ray diffraction and *in situ* in-plane resistivity anisotropy measurements under applied uniaxial stress. We have confirmed that the in-plane resistivity anisotropy below T_S is attributed to the asymmetry in volume fractions of the monoclinic domains, which can be controlled by applying relatively weak uniaxial stress along the tetragonal a or b axis, as was suggested in the previous studies [15,16]. In addition, we found the in-plane resistivity anisotropy above T_S, which is distinct from the onset of the low-temperature monoclinic phase. From the results of the x-ray diffraction and *in situ* resistivity measurements, we have concluded that the in-plane resistivity anisotropy above T_S is induced by a combination of the lattice softening enhanced toward T_S and the application of uniaxial stress. As one of the possibilities, we suggest that the lattice softening and the induced resistivity anisotropy originate from the orbital fluctuation, and that the orbital degree of freedom plays an important role in the structural phase transition in this system.

ACKNOWLEDGMENTS

We are grateful to Y. Takano and Y. Mizuguchi for helpful discussions on the sample preparation. This work was supported by Grants-in-Aid for Young Scientists (B) (Grants No. 25800203 and No. 24740242) from JSPS, Japan. The x-ray diffraction experiments at BL-3A were approved by the Photon Factory Program Advisory Committee (Proposals No. 2012S2-005 and No. 2013G676). The images of the crystal and magnetic structures in this paper were depicted using the software VESTA [30], developed by K. Momma.

[1] Y. Kamihara, T. Watanabe, M. Hirano, and H. Hosono, J. Am. Chem. Soc. **130**, 3296 (2008).

[2] J. Paglione and R. L. Greene, Nat. Phys. **6**, 645 (2010).

[3] N. Ni, M. E. Tillman, J.-Q. Yan, A. Kracher, S. T. Hannahs, S. L. Bud'ko, and P. C. Canfield, Phys. Rev. B **78**, 214515 (2008).

[4] M. Rotter, M. Tegel, and D. Johrendt, Phys. Rev. Lett. **101**, 107006 (2008).

[5] S. Jiang, H. Xing, G. Xuan, C. Wang, Z. Ren, C. Feng, J. Dai, Z. Xu, and G. Cao, J. Phys.: Condens. Matter **21**, 382203 (2009).

[6] C. de la Cruz, Q. Huang, J. W. Lynn, J. Li, W. Ratcliff II, J. L. Zarestky, H. A. Mook, G. F. Chen, J. L. Luo, N. L. Wang *et al.*, Nature (London) **453**, 899 (2008).

[7] J.-H. Chu, J. G. Analytis, K. De Greve, P. L. McMahon, Z. Islam, Y. Yamamoto, and I. R. Fisher, Science **329**, 824 (2010).

[8] S. Kasahara, H. J. Shi, K. Hashimoto, S. Tonegawa, Y. Mizukami, T. Shibauchi, K. Sugimoto, T. Fukuda, T. Terashima, A. H. Nevidomskyy *et al.*, Nature (London) **486**, 382 (2012).

[9] Y. Kim, W. Jung, G. Han, K.-Y. Choi, C.-C. Chen, T. Devereaux, A. Chainani, J. Miyawaki, Y. Takata, Y. Tanaka *et al.*, Phys. Rev. Lett. **111**, 217001 (2013).

[10] Y. Gallais, R. M. Fernandes, I. Paul, L. Chauvière, Y.-X. Yang, M.-A. Méasson, M. Cazayous, A. Sacuto, D. Colson, and A. Forget, Phys. Rev. Lett. **111**, 267001 (2013).

[11] M. Tanatar, E. Blomberg, A. Kreyssig, M. Kim, N. Ni, A. Thaler, S. Bud'ko, P. Canfield, A. Goldman, I. Mazin *et al.*, Phys. Rev. B **81**, 184508 (2010).

[12] C. Dhital, Z. Yamani, W. Tian, J. Zeretsky, A. S. Sefat, Z. Wang, R. J. Birgeneau, and S. D. Wilson, Phys. Rev. Lett. **108**, 087001 (2012).

[13] Y. Mizuguchi and Y. Takano, J. Phys. Soc. Jpn. **79**, 102001 (2010).

[14] W. Bao, Y. Qiu, Q. Huang, M. A. Green, P. Zajdel, M. R. Fitzsimmons, M. Zhernenkov, S. Chang, M. Fang, B. Qian *et al.*, Phys. Rev. Lett. **102**, 247001 (2009).

[15] J. Jiang, C. He, Y. Zhang, M. Xu, Q. Q. Ge, Z. R. Ye, F. Chen, B. P. Xie, and D. L. Feng, Phys. Rev. B **88**, 115130 (2013).

[16] L. Liu, M. Takahashi, T. Mikami, S. Ishida, T. Kakeshita, and S. ichi Uchida, JPS Conf. Proc. **3**, 015035 (2014).

[17] T. Nakajima, S. Mitsuda, T. Nakamura, H. Ishii, T. Haku, Y. Honma, M. Kosaka, N. Aso, and Y. Uwatoko, Phys. Rev. B **83**, 220101 (2011).

[18] T. Nakajima, S. Mitsuda, K. Takahashi, K. Yoshitomi, K. Masuda, C. Kaneko, Y. Honma, S. Kobayashi, H. Kitazawa, M. Kosaka *et al.*, J. Phys. Soc. Jpn. **81**, 094710 (2012).

[19] T. Nakajima, Y. Iguchi, H. Tamatsukuri, S. Mitsuda, Y. Yamasaki, H. Nakao, and N. Terada, J. Phys. Soc. Jpn. **82**, 114711 (2013).

[20] H. C. Montgomery, J. Appl. Phys. **42**, 2971 (1971).

[21] B. F. Logan, S. O. Rice, and R. F. Wick, J. Appl. Phys. **42**, 2975 (1971).

[22] T. Machida, K. Kogure, T. Kato, H. Nakamura, H. Takeya, T. Mochiku, S. Ooi, Y. Mizuguchi, Y. Takano, K. Hirata *et al.*, Phys. Rev. B **87**, 214508 (2013).

[23] Note that the zero-stress measurements shown in Figs. 6(a) and 6(d) were performed after several cooling and heating runs under applied uniaxial stress. On the other hand, the zero-stress measurements shown in Figs. 4(a), 4(c), and 4(d) were performed at the very first stage of the experiment. Therefore the finite resistivity anisotropy in Fig. 6(d) might be due to a small residual stress in the sample. Nevertheless, this small residual stress hardly affects the crystal structure and the resistivity anisotropy above T_s, as shown in Figs. 6(a) and 6(d).

[24] Note that we also observed small peaks at lower angles in the θ scans above T_S, as shown in Fig. 7(a). This has nothing to do with the structural transition to the monoclinic phase, because they are observed even in the tetragonal phase at 0 Pa. They are attributed to small crystal domains with slightly different orientations.

[25] R. M. Fernandes, L. H. VanBebber, S. Bhattacharya, P. Chandra, V. Keppens, D. Mandrus, M. A. McGuire, B. C. Sales, A. S. Sefat, and J. Schmalian, Phys. Rev. Lett. **105**, 157003 (2010).

[26] M. Yoshizawa, D. Kimura, T. Chiba, S. Simayi, Y. Nakanishi, K. Kihou, C.-H. Lee, A. Iyo, H. Eisaki, M. Nakajima *et al.*, J. Phys. Soc. Jpn. **81**, 024604 (2012).

[27] A. M. Turner, F. Wang, and A. Vishwanath, Phys. Rev. B **80**, 224504 (2009).

[28] The resolution of the previous measurements by Kasahara *et al.* is roughly estimated to be $\Delta Q \sim 0.01\,\text{Å}^{-1}$, according to the energy of the incident x ray, the 2θ angle of the reflection, and the peak width above T^*, which are shown in Ref. [8] and its supplemental paper, while that of the present experiment was about $0.005\,\text{Å}^{-1}$. Therefore, if $Fe_{1+\delta}Te$ exhibited a similar degree of broadening, we could observe significant changes in the diffraction profiles.

[29] J.-H. Chu, H.-H. Kuo, J. G. Analytis, and I. R. Fisher, Science **337**, 710 (2012).

[30] K. Momma and F. Izumi, J. Appl. Crystallogr. **41**, 653 (2008).